

# Orientation Dependence of the Intrinsic Anomalous Hall Effect in hcp Cobalt

Eric Roman, Yuriy Mokrousov, and Ivo Souza

Department of Physics, University of California, Berkeley, CA 94720, USA

(Dated: October 26, 2018)

We carry out first-principles calculations of the dependence of the intrinsic anomalous Hall conductivity vector  $\sigma^a$  of hcp Co on the magnetization direction  $\hat{\mathbf{m}}$ . The magnitude of  $\sigma^a$  decreases smoothly from 481 S/cm to 116 S/cm as the magnetization is tilted from the  $c$ -axis to the  $ab$ -plane. This factor-of-four reduction compares well with measurements on single crystals, while the angular average  $\langle \sigma^a \cdot \hat{\mathbf{m}} \rangle = 226$  S/cm is in excellent agreement with the value of 205 S/cm measured in polycrystalline films. The strong anisotropy of  $\sigma^a$  is a consequence of spin-orbit induced changes in the electron states near the Fermi level as the magnetization is rotated.

PACS numbers: 75.30.Gw, 75.30.-m, 72.15.Gd, 78.20.Ls

The Hall effect in ferromagnets has two contributions. The ordinary Lorentz-force part, which is proportional to the magnetic field for weak fields, and an “anomalous” part, which depends on the magnetization. A theory of the anomalous Hall effect (AHE) was put forth by Karplus and Luttinger [1], who showed that a Hall current perpendicular to the electric field and odd under magnetization reversal is established in a ferromagnetic crystal as a result of the spin-orbit interaction (SOI).

The link between the AHE and the SOI became consensual, but a long debate ensued on whether the relevant SOI is associated with the crystalline potential (intrinsic) or with impurity atoms (extrinsic). The asymmetric impurity scattering of the spin-polarized charge carriers (skew-scattering) leads to a linear dependence of the anomalous Hall resistivity  $\rho_{yx}^a = E_y/j_x$  on the longitudinal resistivity  $\rho_{xx}$ ; an additional scattering process, side-jump, yields the same scaling  $\rho_{yx}^a \propto \rho_{xx}^2$  as the intrinsic Karplus-Luttinger mechanism. For a review see Ref. 2.

Unlike the extrinsic contributions, which depend on the details of the impurity potential, the Karplus-Luttinger anomalous Hall conductivity (AHC) can be evaluated from the band structure of the crystal [2, 3]:

$$\sigma_{ij}^a = -\frac{e^2}{\hbar} \int_{\text{BZ}} \frac{d^3k}{(2\pi)^3} \sum_n f_{n\mathbf{k}} \Omega_{n\mathbf{k},ij}, \quad (1)$$

where  $f_{n\mathbf{k}}$  is the Fermi-Dirac distribution function and  $\Omega_{n,ij}(\mathbf{k})$  is the Berry curvature tensor of each cell-periodic spinor Bloch state  $|u_{n\mathbf{k}}\rangle$ . First-principles calculations for Fe, Co, Ni [3, 4, 5], SrRuO<sub>3</sub> [6] and Mn<sub>5</sub>Ge<sub>3</sub> [7] have consistently found good agreement with room-temperature experiments, establishing the importance of the intrinsic mechanism.

Recent experiments have focused on isolating the different contributions to the AHE [7, 8, 9]. Skew-scattering can be separated from the other two terms by fitting the measured anomalous Hall resistivity to the form

$$\rho_{yx}^a = a\rho_{xx} + b\rho_{xx}^2, \quad (2)$$

where  $b = \sigma_{xy}^a + b^{\text{SJ}}$ . The coefficients  $a$  (skew-scattering) and  $b$  (intrinsic plus side-jump) can be read off a plot of  $\rho_{yx}^a/\rho_{xx}$  versus  $\rho_{xx}$ , where  $\rho_{xx}$  is varied through doping or temperature changes.

In this Letter, we present a detailed first-principles study of the orientation dependence of the intrinsic AHE. Anisotropy in the AHE has been measured in single crystals of the ferromagnetic elements (hcp Co [10], hcp Gd [11], fcc Ni [12], and bcc Fe [13]), and more recently in ferromagnetic compounds [14, 15, 16]. On the theoretical side there has been little progress beyond the basic phenomenological description. To our knowledge, the only attempt at a microscopic model has been the tight-binding study of Ref. 14. Because the AHC is very sensitive to fine details in the band structure [3, 4, 6], a quantitative *ab initio* theory of anisotropy is highly desirable. It is also not obvious that the phenomenological description of magnetocrystalline anisotropy [17, 18] applies to the AHC given by Eq. (1). The Berry curvature undergoes strong and rapid variations in  $k$ -space, with sharp peaks and valleys from avoided crossings near the Fermi level [3, 4, 6]. It has been argued that such behavior cannot be described perturbatively [3], and that it often gives rise to a complex or even irregular behavior of the AHC as a function of exchange splitting and Fermi level position [6]. This raises the possibility that the orientation dependence of  $\sigma_{ij}^a$  may also not be smooth. We find instead that in hcp Co it is strong but remarkably smooth, and can be described by a phenomenological power-series expansion. The calculated anisotropy accounts for the experimental observations in both single crystals (angular dependence) and polycrystalline films (angular average).

We begin by reviewing the phenomenology [17, 18]. Electrical conduction in ferromagnets is described by a magnetization-dependent conductivity tensor:  $J_i = \sigma_{ij}(\mathbf{M})E_j$ , where  $i, j$  are Cartesian indices. The Onsager relation  $\sigma_{ij}(\mathbf{M}) = \sigma_{ji}(-\mathbf{M})$  implies that the symmetric ( $\sigma_{ij}^s$ ) and antisymmetric ( $\sigma_{ij}^a$ ) parts of  $\sigma_{ij}$  are respectively even and odd functions of the magnetization  $\mathbf{M}$ . The current density  $\mathbf{J}$  is therefore comprised of an even (Ohmic) part  $\mathbf{J}^s$  and an odd (Hall) part  $\mathbf{J}^a$ . The Hall current

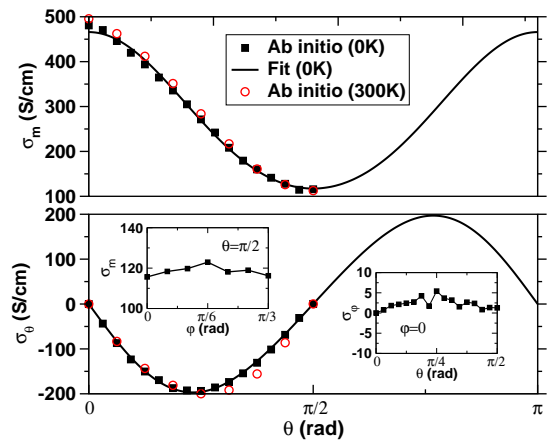


FIG. 1: (Color online.) Evolution of the components of the anomalous Hall conductivity parallel ( $\sigma_m$ ) and perpendicular ( $\sigma_\theta$ ) to the magnetization [Eq. (3)] as  $\mathbf{M}$  is tilted by  $\theta$  from the  $c$ -axis towards the  $a$ -axis. The solid lines are fits to the first-principles data, as described in the text. The left and right insets show respectively  $\sigma_m(\pi/2, \varphi)$ , and  $\sigma_\theta(\theta, 0)$ .

reads  $\mathbf{J}^a = \mathbf{E} \times \boldsymbol{\sigma}^a$ , where  $\sigma_k^a = (1/2)\epsilon_{ijk}\sigma_{ij}^a$ .  $\mathbf{J}^a$  is perpendicular to  $\mathbf{E}$  but not necessarily to  $\mathbf{M}$ , since  $\boldsymbol{\sigma}^a$  and  $\mathbf{M}$  may not be collinear. This is the situation in single crystals, where  $\boldsymbol{\sigma}^a \parallel \mathbf{M}$  only when  $\mathbf{M}$  points along certain high-symmetry directions.

To characterize the anisotropy we write  $\boldsymbol{\sigma}^a$  as

$$\boldsymbol{\sigma}^a = \sigma_m \hat{\mathbf{m}} + \sigma_\theta \hat{\boldsymbol{\theta}} + \sigma_\varphi \hat{\boldsymbol{\varphi}}, \quad (3)$$

where  $\theta$  and  $\varphi$  are respectively the polar and azimuthal angles of  $\mathbf{M} = M\hat{\mathbf{m}}$ . In macroscopically isotropic systems such as polycrystals  $\boldsymbol{\sigma}^a \parallel \mathbf{M}$ , i.e.,  $\sigma_\theta = \sigma_\varphi = 0$ . The orientation dependence in hcp single crystals is given to third order in a spherical-harmonic expansion by [19]

$$\begin{cases} \sigma_1^a = c_{11}\bar{Y}_{11} + c_{31}\bar{Y}_{31} \\ \sigma_2^a = c_{11}\bar{Y}_{1,-1} + c_{31}\bar{Y}_{3,-1} \\ \sigma_3^a = c_{10}\bar{Y}_{10} + c_{30}\bar{Y}_{30} \end{cases}, \quad (4)$$

where  $\bar{Y}_{lm}(\theta, \varphi)$  are real spherical harmonics. Because  $\sigma_3^a$  is independent of  $\varphi$ , while  $\sigma_1^a$  and  $\sigma_2^a$  have respectively cosine and sine dependences,  $\boldsymbol{\sigma}^a$  and  $\mathbf{M}$  share the same azimuthal angle, and their polar-angle mismatch is independent of  $\varphi$ . Thus  $\sigma_{m,\theta} = \sigma_{m,\theta}(\theta)$  and  $\sigma_\varphi = 0$ .

We have carried out fully-relativistic band-structure calculations for hcp and fcc Co at the experimental lattice constants of 4.74 and 6.68 bohr respectively, using the PWSCF code [20]. The pseudopotential was generated using similar parameters as in Ref. 4. The plane-wave basis cutoff was set at 140 Ry, and the exchange-correlation functional,  $k$ -point sampling, and Fermi smearing used in the self-consistent calculation are the same as in Ref. 4. The integral in Eq. (1) was evaluated using a Wannier-interpolation scheme [4] to sample efficiently the Brillouin zone over a  $125 \times 125 \times 125$  uniform  $k$ -point mesh

TABLE I: Anomalous Hall conductivity  $|\boldsymbol{\sigma}^a| = \sigma_m$  in S/cm for selected high-symmetry orientations of the magnetization in hcp and fcc Co. The AHC of polycrystalline samples is calculated as an orientational average (see text).

Co	Orientation	Calc.	Expt.
hcp	$c$ -axis	481	683 <sup>a</sup>
	$ab$ -plane	116	232 <sup>a</sup>
	Polycrystal	226	205 <sup>b</sup> , 275 <sup>c</sup>
fcc	[001]	249	
	[110]	218	
	[111]	234	

<sup>a</sup>Reference 10

<sup>b</sup>Reference 8

<sup>c</sup>Reference 22

( $200 \times 200 \times 200$  for fcc Co), with a  $5 \times 5 \times 5$  adaptively refined mesh around the points where the magnitude of the Berry curvature exceeded  $10 \text{ \AA}^2$ .

The AHC of hcp Co was calculated for several orientations of the cell-averaged magnetization [21] in the  $ac$ -plane ( $\varphi = 0$ ). The tilting angle  $\theta$  was increased from 0 ( $\mathbf{M} \parallel c$ -axis) to  $\pi/2$  ( $\mathbf{M} \parallel a$ -axis) in steps of  $\pi/32$ , and for each step the vector  $\boldsymbol{\sigma}^a(\theta, \varphi)$  was calculated. Fig. 1 contains the numerical results:  $\sigma_m(\theta, 0)$  and  $\sigma_\theta(\theta, 0)$  are shown in the main panels, while the insets contain additional data which confirms the absence of (or very weak) basal-plane anisotropy. The vectors  $\boldsymbol{\sigma}^a$  and  $\mathbf{M}$  start out parallel, but as  $\mathbf{M}$  begins to tilt away from the  $c$ -axis  $\boldsymbol{\sigma}^a$  lags behind ( $\sigma_\theta < 0$ ), and they become parallel again upon reaching the basal plane. The AHC is strongly anisotropic, decreasing in magnitude by a factor of  $481/116 \simeq 4.1$  between  $\theta = 0$  and  $\theta = \pi/2$ . This is in reasonable agreement with the ratio of 2.93 measured in single crystals at 290 K [10]. While strong, the angular dependence of  $\boldsymbol{\sigma}^a$  is smooth, and can be described by Eq. (4). A least-squares fitting to the data yields, in S/cm,  $c_{10} = 951.5$ ,  $c_{11} = -204.1$ ,  $c_{30} = 1.2$ , and  $c_{31} = 38.4$ , producing the solid-line curves in Fig. 1.

We now turn to the comparison with the measurements on polycrystalline films [8]. The films were magnetized along the growth direction by an applied field; assuming randomly oriented crystallites, each with a bulk-like Hall current density  $\mathbf{J}^a(\theta, \varphi)$ , the net Hall current density in the films can be estimated by performing an orientational average:  $\langle \mathbf{J}^a \rangle = \mathbf{E} \times \langle \boldsymbol{\sigma}^a \rangle$ . Because  $\boldsymbol{\sigma}^a$  displays azimuthal isotropy, it suffices to average Eq. (3) over  $\theta$  for fixed  $\varphi$ . The average of  $\sigma_\theta$  vanishes (see Fig. 1), resulting in an isotropic AHC  $\langle \boldsymbol{\sigma}^a \rangle = \langle \sigma_m \rangle \hat{\mathbf{m}}$  of magnitude  $\sigma_{\text{poly}}^a = \int_0^{\pi/2} \sigma_m(\theta) \sin \theta d\theta = 226 \text{ S/cm}$ . This should be compared with the value  $b = 205 \text{ S/cm}$  obtained in Ref. 8 by fitting the experimental data to Eq. (2). The experiment does not discriminate between the intrinsic and side-jump components of  $b$ , but the close agreement with

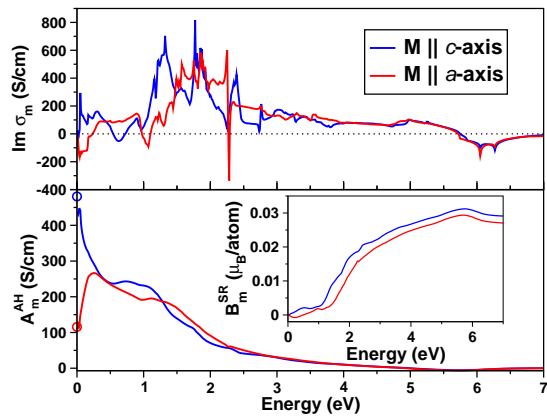


FIG. 2: (Color online.) Upper panel: MCD spectrum for two magnetization directions. Lower panel: Cumulative contribution to the AHC from the spectrum above energy  $\hbar\omega$ . The circles denote the AHC calculated directly from Eq. (1). Inset: Cumulative contribution to the self-rotation part of the orbital magnetization from the spectrum below  $\hbar\omega$ .

the calculated  $\sigma_{\text{poly}}^a$  reinforces the conclusion [8] that the former dominates. Table I summarizes the comparison between our calculations and experiments.

Next we discuss the origin of the strong anisotropy. The AHE of uniaxial crystals is anisotropic to first order in an expansion in powers of the magnetization [19], while in cubic crystals anisotropy appears only in third-order [12], and is expected to be much weaker. For example, the AHC of fcc Co changes by less than 10% as a function of the magnetization direction (Table I). Perhaps more surprising is the fact that the AHE in hcp Co appears to be considerably more anisotropic than both the magneto-optical spectrum [23] and the orbital magnetization [24, 25]. This is intriguing because the three phenomena are related by linear sum rules [26], and hence anisotropy appears at the same order.

The sum rules read  $\langle \omega^{-1} \text{Im} \sigma^a \rangle_\omega = (\pi/2) \sigma^a(\omega = 0)$  and  $\langle \text{Im} \sigma^a \rangle_\omega = (\pi e c / \hbar) \mathbf{M}_{\text{SR}}^{(1)}$ , where  $\langle f \rangle_\omega = \int_0^\infty f(\omega) d\omega$ .  $\sigma^a(\omega = 0)$  is the dc AHC; at finite frequencies  $\sigma^a$  acquires an imaginary part which describes the differential absorption of right and left circularly-polarized light, or magnetic circular dichroism (MCD). The first sum rule expresses the AHC in terms of the first inverse moment of the MCD spectrum. The second relates  $\mathbf{M}_{\text{SR}}^{(1)}$ , the “gauge-invariant self-rotation” part of the orbital magnetization [26], to the zero-th spectral moment.

The absorptive part of  $\sigma_m(\omega)$  is plotted in the upper panel of Fig. 2 for  $\theta = 0, \pi/2$ . The lower panel shows  $A_m^{\text{AH}}(\omega) = \frac{2}{\pi} \int_0^{\omega_{\text{max}}} \frac{1}{\omega'} \text{Im} \sigma_m(\omega') d\omega'$ . For  $\omega_{\text{max}} \rightarrow \infty$  (in practice we use  $\omega_{\text{max}} = 7$  eV)  $A_m^{\text{AH}}(0) = \sigma_m(\omega = 0)$ , so that  $A_m^{\text{AH}}(\omega > 0)$  is the cumulative contribution to the AHC from optical transitions above  $\omega$ . While for either orientation there are sizeable contributions to the AHC up to  $\omega \sim 3.5$  eV, its orientation dependence is

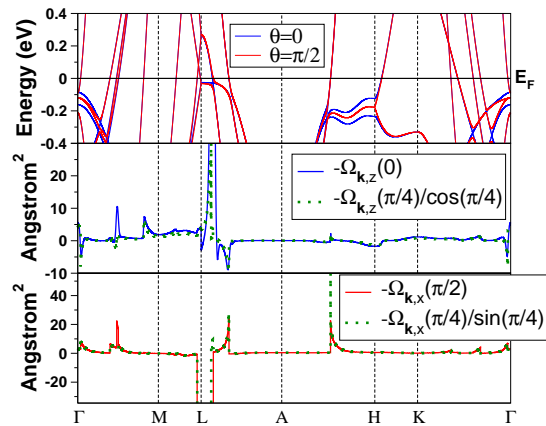


FIG. 3: (Color online.) Upper panel: Energy bands close to the Fermi level for  $\mathbf{M} \parallel c$ -axis ( $\theta = 0$ ) and  $\mathbf{M} \parallel a$ -axis ( $\theta = \pi/2$ ). Middle and lower panels:  $k$ -space Berry curvature  $\Omega_{\mathbf{k}}(\theta)$  for  $\theta = 0$ ,  $\theta = \pi/2$ , and  $\theta = \pi/4$ . The full height of the resonance peaks near the  $L$ -point is of the order of  $10^3 \text{ \AA}^2$ .

concentrated below 0.3 eV. At these low frequencies the MCD spectrum changes sign between  $\theta = 0$  and  $\theta = \pi/2$ . This difference gets magnified in the AHC via the inverse-frequency weight factor, producing the bifurcation below 0.3 eV of the two  $A_m^{\text{AH}}(\omega)$  curves. All frequencies are equally weighted in the orbital moment sum rule, which as a result is more isotropic. This is seen in the inset, where we plot  $B_m^{\text{SR}}(\omega) = \frac{V_c \hbar}{2\pi e c} \int_0^\omega \text{Im} \sigma_m^a(\omega') d\omega'$ , the cumulative contribution below  $\omega$  to the gauge-invariant self-rotation per atom.

The origin of the low-frequency anisotropy can be seen in Fig. 3. The upper panel displays the energy bands for the two magnetization directions. Rotating  $\mathbf{M}$  from the  $c$ -axis to the  $a$ -axis in the presence of the SOI turns various band crossings into avoided crossings and vice-versa. When this occurs close to the Fermi level the Berry curvature along  $\mathbf{M}$  can flip sign in the process, while retaining a large magnitude. This is what happens near the  $L$ -point, as seen in the middle and lower panels, where we plot  $-\Omega_{\mathbf{k}} \cdot \hat{\mathbf{m}}$  for the two orientations ( $\Omega_{\mathbf{k},k} = (1/2)\epsilon_{ijk} \sum_n f_{n\mathbf{k}} \Omega_{n\mathbf{k},ij}$  is the total Berry curvature at  $\mathbf{k}$ ). The sensitivity of the AHC to changes in the electron states near  $E_F$  may also be understood from the fact that  $\sigma^a$  can be recast as a Fermi surface integral [5, 27], whereas the orbital magnetization truly depends on all occupied states.

How can the spiky behavior of  $\Omega_{\mathbf{k}}$  be reconciled with the smooth angular dependence displayed by  $\sigma^a(\theta)$  in Fig. 1? According to the phenomenological expansion (4),  $\sigma_i^a \propto M_i$  to leading order ( $i = x, y, z$ ). This will be the case for the AHC given by Eq. (1) provided that  $\Omega_{\mathbf{k},i} \propto M_i$  at each  $\mathbf{k}$ . This proportionality holds reasonably well even around strong resonance peaks, judging from the comparison in Fig. 3 between  $\Omega_{\mathbf{k}}$  calculated at

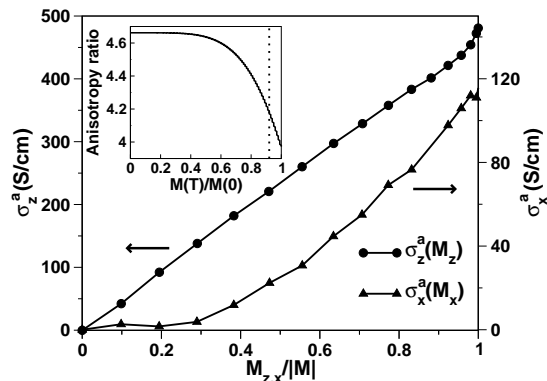


FIG. 4: Evolution of  $\sigma^a$  as the magnetization is rotated in the  $ac$  plane, plotted as  $\sigma_z^a(\cos\theta)$  and  $\sigma_x^a(\sin\theta)$ . Inset: Anisotropy ratio  $\sigma_z^a(\theta=0)/\sigma_x^a(\theta=\pi/2)$  versus the reduced magnetization, according to the spin-fluctuation model. The dotted line denotes the approximate location of the hcp  $\rightarrow$  fcc transition.

$\theta = \pi/4$  and at  $\theta = 0, \pi/2$ .

We end with a discussion of temperature effects. The AHC hardly changes as the Fermi-smearing temperature in Eq. (1) is varied from 0 K to 300 K (Fig. 1). This agrees with the constancy of the coefficient  $b$  of polycrystalline films in the range 78-350 K [8]. The angular dependence of the AHC can also give rise to a temperature dependence, via long-wavelength thermal fluctuations in  $\hat{\mathbf{m}}$  [7]. According to this model, if  $\sigma_i^a(T=0)$  changes linearly with  $M_i$  upon rotating  $\mathbf{M}$  then  $\sigma^a(T) = [M(T)/M(0)]\sigma^a(T=0)$ , which seems to explain the temperature dependence in  $\text{Mn}_5\text{Ge}_3$  [7]. Fig. 4 shows that in hcp Co  $\sigma_z^a$  depends linearly on  $M_z$ , while the  $\sigma_x^a(M_x)$  curve is significantly nonlinear (note that  $|c_{31}/c_{11}| \gg |c_{30}/c_{10}|$ ). As a result, the  $a$ -axis AHC should decrease with  $T$  faster than  $M(T)$ , producing an increase with temperature of the ratio  $\sigma_z^a(\theta=0)/\sigma_x^a(\theta=\pi/2)$ . An estimate of the magnitude of this effect can be obtained using the “ $l(l+1)/2$  power law” [28, 29] for the coefficients  $c_{lm}(T)$  (see Ref. 19 for details). The result, shown in the inset of Fig. 4, is a 17% increase between 0 K and  $T_c$ . This is a sufficiently large effect that is should be observable in principle, but in practice it is preempted by the phase transformation into the fcc structure at 695 K, well below  $T_c = 1400$  K [30].

In summary, we have shown by means of first-principles calculations that the intrinsic mechanism for the AHE describes quantitatively the observed strong angular dependence in hcp Co single crystals. The key role of near-degeneracies across the Fermi level was elucidated, and the AHE of polycrystalline Co films was reproduced by averaging the single-crystal Hall conductivity over all magnetization directions. Further experimental and theoretical studies of the orientation dependence of the AHE are needed. For example, very little is known about the

anisotropy of the skew-scattering contribution [16].

The authors wish to thank David Vanderbilt, Jonathan Yates, and Xinjie Wang for fruitful discussions. This work was supported by NSF Grant No. DMR 0706493. Computational resources have been provided by NERSC.

- 
- [1] R. Karplus and J. M. Luttinger, Phys. Rev. **95**, 1154 (1954).
  - [2] N. Nagaosa et al., arXiv:0904.4154 (2009).
  - [3] Y. Yao et al., Phys. Rev. Lett. **92**, 037204 (2004).
  - [4] X. Wang, J. R. Yates, I. Souza, and D. Vanderbilt, Phys. Rev. B **74**, 195118 (2006).
  - [5] X. Wang, D. Vanderbilt, J. R. Yates, and I. Souza, Phys. Rev. B **76**, 195109 (2007).
  - [6] Z. Fang et al., Science **302**, 92 (2003).
  - [7] C. Zeng, Y. Yao, Q. Niu, and H. H. Weiering, Phys. Rev. Lett. **96**, 037204 (2006).
  - [8] J. Kötzler and W. Gil, Phys. Rev. B **72**, 060412(R) (2005).
  - [9] Y. Tian, L. Ye, and X. Jin, arXiv:0903.5360 (2009).
  - [10] N. V. Volkenshtein, G. V. Fedorov, and V. P. Shirokovskii, Phys. Met. Metallogr. **11**, 151 (1961).
  - [11] R. S. Lee and S. Legvold, Phys. Rev. **162**, 431 (1967).
  - [12] T. Hiraoka, J. Sci. Hiroshima Univ., Ser. A-II **32**, 153 (1968).
  - [13] A. A. Hirsch and Y. Weissman, Phys. Lett. **44A**, 239 (1973).
  - [14] K. Ohgushi, S. Miyasaka, and Y. Tokura, J. Phys. Soc. Jpn. **75**, 013710 (2006).
  - [15] B. C. Sales, R. Jin, and D. Mandrus, Phys. Rev. B **77**, 024409 (2008).
  - [16] J. Stankiewicz and K. P. Skokov, Phys. Rev. B **78**, 214435 (2008).
  - [17] R. R. Birss, *Symmetry and Magnetism* (North-Holland, 1964).
  - [18] C. M. Hurd, Adv. Phys. **23**, 315 (1974).
  - [19] See supplementary material.
  - [20] S. Baroni et al., <http://www.quantum-espresso.org>.
  - [21] Because of the SOI, the spin density  $\sigma(\mathbf{r})$  is not strictly collinear within the crystalline cell. In hcp Co we find  $|\int_{\text{cell}} d^3r \sigma(\mathbf{r})| = 3.20 \mu_B$ , while  $|\int_{\text{cell}} d^3r |\sigma(\mathbf{r})| = 3.53 \mu_B$ .
  - [22] N. V. Volkenshtein and G. V. Fedorov, Soviet Phys. - JETP **11**, 48 (1960).
  - [23] D. Weller et al., Phys. Rev. Lett. **72**, 2097 (1994).
  - [24] J. Trygg, B. Johansson, O. Eriksson, and J. M. Wills, Phys. Rev. Lett. **75**, 2871 (1995).
  - [25] D. Ceresoli, U. Gerstmann, A. P. Seitsonen, and F. Mauri, arXiv:0904.1988 (2009).
  - [26] I. Souza and D. Vanderbilt, Phys. Rev. B **77**, 054438 (2008).
  - [27] F. D. M. Haldane, Phys. Rev. Lett. **93**, 206602 (2004).
  - [28] C. Zener, Phys. Rev. **96**, 1355 (1954).
  - [29] H. B. Callen and E. Callen, J. Phys. Chem. Solids **27**, 1271 (1966).
  - [30] The AHC of polycrystalline Co has been found to drop at the hcp  $\rightarrow$  fcc transition temperature from  $\sim 1320$  S/cm to  $\sim 660$  S/cm [I. A. Tsoukalas, Phys. Stat. Sol. (a) **23**, K41 (1974)]. These values seem inconsistent with Table I.